



HAL
open science

On the Effective Accuracy of Spectral-Like Optimized Interpolation Schemes for Computational Acoustics

G Cunha, S Redonnet

► **To cite this version:**

G Cunha, S Redonnet. On the Effective Accuracy of Spectral-Like Optimized Interpolation Schemes for Computational Acoustics. *Journal of Computational Physics*, 2014, 263, pp.222-232. 10.1016/j.jcp.2014.01.024 . hal-01080153

HAL Id: hal-01080153

<https://hal.science/hal-01080153>

Submitted on 4 Nov 2014

HAL is a multi-disciplinary open access archive for the deposit and dissemination of scientific research documents, whether they are published or not. The documents may come from teaching and research institutions in France or abroad, or from public or private research centers.

L'archive ouverte pluridisciplinaire **HAL**, est destinée au dépôt et à la diffusion de documents scientifiques de niveau recherche, publiés ou non, émanant des établissements d'enseignement et de recherche français ou étrangers, des laboratoires publics ou privés.

On the Effective Accuracy of Spectral-Like Optimized Interpolation Schemes for Computational Acoustics

G.Cunha*

Laboratório de Combustão e Propulsão - INPE, Dutra Km 40, Cachoeira Paulista - SP, Brasil, CEP 12.630-000.

S.Redonnet

Department of CFD and Aeroacoustics - Onera (French Aerospace Lab), BP 72 - Avenue Division Leclerc, Châtillon, 92322, France.

Abstract

The present work constitutes a fraction of a more extensive study that is devoted to numerical methods in acoustics. More precisely, we address here the interpolation process, which is more and more frequently used in Computational Acoustics - whatever it is for enabling multi-stage hybrid calculations, or for easing the proper handling of complex configurations via advanced techniques such as Chimera grids or Immersed Boundary Conditions. In that regard, we focus here on high-order interpolation schemes, so as to analyze their intrinsic features and to assess their effective accuracy. Taking advantage of specific advances that had been previously achieved by the present authors regarding centered and standard high-order interpolation schemes, we here focus on spectral-like optimized and/or noncentered ones. The latter are analyzed thoroughly thanks to dedicated theoretical developments, which allow highlighting better what their strengths and weaknesses are. Among others, the various ways such interpolation schemes can degrade acoustic signals they are applied to are carefully investigated from a theoretical point-of-view, before they are numerically assessed thanks to several academic test cases. Besides that, specific criteria that could help in optimizing interpolation schemes better are provided, along with generic rules about how to minimize the signal degradation induced by existing interpolation schemes, in practice. Finally, conclusions are drawn about the effective accuracy one can expect from those noncentred and/or spectral-like optimized interpolations.

Keywords: Noncentered interpolation, centered interpolation, high-order, spectral-like optimization, spurious modes generation, computational acoustics

1. Introduction

Nowadays, many fields of research focus on the modeling of noise phenomena, which finds plenty of applications within numerous domains. Indeed, adequately modeling and predicting noise phenomena can help in improving existing technologies, such as reducing the noise annoyances by industrial products (aircraft, trains or cars, wind turbines, computers, etc.). It can also help optimizing specific acoustic-based devices, such as those used for non destructive control, non intrusive medical imaging, seismic monitoring, and so on. Finally, it can facilitate the emergence of new technologies, such as alternative and innovative acoustic-based devices (sensor less tactile screens, ultra-sound medical curative techniques, etc.). On another hand, since acoustic is a complex discipline, researchers are now bounded to make an intensive use of numerical simulation, which constitutes a powerful mean of investigation, when coming in complement to the experimentation.

This, however, requires the continuous development and improvement of modeling and solving techniques that can account for all mechanisms underlying the noise generation and/or propagation phenomena. Indeed, noise finds its

*Corresponding author.

Email addresses: `Guilherme.Cunha@lcp.inpe.br` (G.Cunha), `stephane.redonnet@onera.fr` (S.Redonnet)

origin in numerous source mechanisms such as structural vibrations, fluidic motions, flow interactions with structures, gas combustion or explosions, and so on. Once they have been generated by these sources, acoustic waves propagate within the surrounding environment, which is generally constituted with one or several media of various complexity (e.g. comprising solid bodies and/or medium heterogeneity, etc.). During such propagation phase, acoustic waves may thus be submitted to numerous and important alterations in terms of amplitude, phase or frequency, which all result from mechanisms as diverse as reflection and diffraction effects by solid structures, convection by fluidic motions, refraction and diffusion by the medium heterogeneity (turbulence, velocity of temperature gradients, etc.), absorption by the medium viscosity, and so on.

Many of the acoustic generation processes and most of the acoustic propagation mechanisms are relevant to the physics of fluid dynamics, and can thus be simulated by numerically solving the Navier-Stokes equations. However, the specificity of acoustic phenomena implies that such solving must be achieved following very precise strategies. In particular, this is what led to the emergence of Computational AeroAcoustics (CAA), a scientific discipline that rapidly progressed over the past twenty years. Among others, such discipline promoted the development of highly-accurate numerical schemes, which minimal dissipation and dispersion properties are mandatory for acoustic waves to be correctly simulated over long propagation distances and time durations [1]. As an illustration, given their higher accuracy and, thus, ability to simulate wave-like phenomena on coarser grids [2], high-order Finite-Difference (FD) methods have emerged as a valuable alternative to more traditional low-order methods that are usually employed in other disciplines (e.g. Computational Fluid Dynamics, CFD).

At the present time, however, and despite of the continuous development of computational tools and resources, it is still very challenging to simulate aeroacoustic problems following a direct manner, i.e. via a single calculation. As an example, except in particular situations, e.g. academic configurations, it is nearly impossible to compute simultaneously both the acoustic generation and propagation phenomena, which underlying mechanisms generally differ by their intrinsic characteristics (such as energy and length scales of phenomena involved, etc.).

Therefore, in most practical cases, aeroacoustic problems are solved following a hybrid manner [3, 4, 5, 6, 7], according to which the overall problem is partitioned into several sub-problems, the latter being numerically simulated using the most adapted strategy, that is, the one offering the best trade-off between accuracy and CPU cost.

Such a hybrid scenario however implies that the various sub-problems are linked (or coupled) altogether, which generally requires that a data transfer is achieved between them. Needless to say, such a data transfer between two stages of a hybrid method must be conducted in a conservative fashion, that is to say, without leading to information loss or duplication. In particular, and because of the mismatches between the discrete formulations associated with all various stages, such a data transfer generally relies on space and/or time interpolation techniques.

On another hand, and from a more global perspective, it appears that interpolation techniques are more and more extensively used for the solving of practical acoustic problems, whatever the latter are addressed following a direct or a hybrid approach. As an example, for practical applications involving complex geometries that cannot be easily handled via a single body-fitted mesh, use is often made of Chimera techniques, which relies on elementary overset-grids that overlap each other, and that are linked altogether via interpolations [2, 3, 8]. In addition, many advanced computational techniques now used within an aeroacoustic context (e.g. multi-size-mesh / multi-time-step techniques [9], immersed boundary methods [10, 11], etc.) also rely on space and/or time interpolation processes. It is clear however that, for not jeopardizing the entire aeroacoustic calculation they are part of, all these interpolation operations must preserve the accuracy of data, at least as much as the highly-accurate numerical schemes to be used do.

On that stage, one can recall that the literature abounds in studies that focused on interpolation techniques, whatever the latter are of low or high order-of-accuracy. In particular, some of these works [2, 10, 12, 13] had highlighted a major side-effect of the interpolation process, which is the so-called signal degradation such process may induce onto that part of the interpolated data which frequency (in terms of wavenumber) is high. With the view of minimizing such a side-effect, some authors have proposed innovative interpolation schemes, either of centered [2, 10] or noncentered [10, 12] nature, to be optimized in a spectral-like sense, that is, in the wavenumber space.

The point is that, as first demonstrated in [13], when interpolated, a signal may not solely be subjected to a degradation of its higher frequency contents, but it can also suffer from additional alterations, to occur over the whole spectrum, because of the so-called *spuriousing* and subsequent *aliasing* phenomena. Since none of the referred studies had provided a thorough analysis of these two specific side-effects, one could legitimately wonder how spectral-like optimized interpolation schemes might effectively behave when subjected to them.

Recently, the present authors have proposed an original formalism [14], which unifies all elements of the interpola-

tion theory, allowing to characterize both the spurious and the aliasing phenomena, as well as to predict their impact in terms of signal degradation. Additionally, such formalism made it possible to assess better high-order standard interpolation schemes [14]. It appeared thus natural to make use of both the development made and the experience gained on that matter for assessing also spectral-like optimized schemes, either of centered [2, 10] or noncentered [10, 12] nature. This is what motivated the present study, and constitutes the subject of the present article.

2. Interpolation Schemes

As was said above, the present work relies on a dedicated formalism [14] that was specifically developed by the present authors for studying interpolation techniques. Such formalism, which is briefly recalled in the [Appendix A](#), relies on the theoretical study of 1D explicit interpolations associated with uniformly discretized donor grids. This choice can be justified by the following reasons:

1. Any multidimensional interpolation can be written as a tensorization of mono-dimensional ones [15].
2. In multidimensional problems, implicit (compact) interpolation methods do not present enough trade-offs, if one compares the complexity of their implementation with respect to the accuracy gain they effectively offer [2].
3. Interpolations are generally achieved in the computational domain (Cartesian grid) rather than in the physical one (curvilinear grid) [16].

Let us then consider a given one-dimensional interpolation stencil built from uniformly spaced points, such as the one depicted in [Figure 1](#). Here, x indicates any position included in the interval $[x_n, x_{n+1}[$ to be covered by the interpolation stencil, which first and last points are indexed by J_{min} and J_{max} (both included in \mathbb{Z}) respectively.

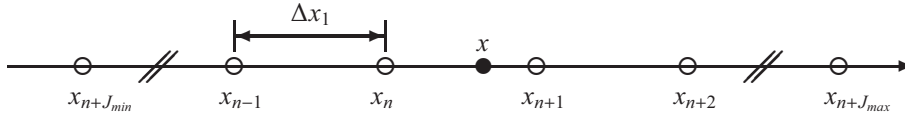


Figure 1: A given receiver point, x , and its associated $|J_{max}|+|J_{min}|+1$ donor points, positioned along a one-dimensional interpolation stencil.

Without a loss of generality, we can assume that the stencil points correspond to a set of donor points associated with a uniform grid to be defined as $x_n = n\Delta x_1$, with $n \in \mathbb{Z}$ and Δx_1 the discretization step. Analogously, x can be seen as an interpolation point associated with a given receiver grid, the latter of which being defined such that $x = m\Delta x_2 + d$, with $m \in \mathbb{Z}$ and $d \in [-\Delta x_1/2, \Delta x_1/2[$ ¹. For any continuous function, $f : \mathbb{R} \rightarrow \mathbb{R}$, its corresponding interpolated function can then be written as:

$$\mathcal{I}[f](x) = \sum_{n=-\infty}^{+\infty} \mathbf{1}_{[0,1[}\left(\frac{x}{\Delta x_1} - n\right) \sum_{j=J_{min}}^{J_{max}} S_j \left(\frac{x}{\Delta x_1} - n\right) f((n+j)\Delta x_1), \quad (1)$$

where $\mathbf{1}_{[0,1[}(\cdot)$ is the identity function,

$$\mathbf{1}_{[0,1[}(x) = \begin{cases} 1, & \text{if } x \in [0, 1[, \\ 0, & \text{if } x \notin [0, 1[. \end{cases} \quad (2)$$

and S_j are the interpolation schemes coefficients, which respective values are still to be evaluated.

¹In the forthcoming sections, the subscript $i \in \{1, 2\}$ associated with a given variable indicates on which grid such variable is considered, that is, donor, $i = 1$, or receiver, $i = 2$. Additionally, unless stated otherwise, $d = 0$ (see [Appendix B](#)).

At this stage, one can first precise that, for avoiding Equation (1) to turn into the extrapolation operator, it is here imposed that $[x_n, x_{n+1}]$ is included in $[x_{n+J_{min}}, x_{n+J_{max}}]$. One can also notice that the particular case of a centered interpolation scheme is met when $[x_n, x_{n+1}]$ corresponds to the central interval included in $[x_{n+J_{min}}, x_{n+J_{max}}]$. Otherwise, the interpolation operator is of noncentered kind. Finally, in the present work, 'Lagrange interpolations' will be referred to as 'standard interpolations'. More particularly, the $(|J_{max}| + |J_{min}| + 1)$ th-order Lagrange interpolation is obtained by setting $S_j(\cdot) = P_j(\cdot)$, $\forall j \in \{J_{min}, \dots, 0, 1, \dots, J_{max}\}$, with

$$P_j(x) = \prod_{p=J_{min}, p \neq j}^{J_{max}} \frac{x - p}{j - p}. \quad (3)$$

3. Interpolation Process and Signal Degradation - Brief Reminder

As was said above, in order to successfully achieve aeroacoustic calculations, it is mandatory to make use of highly accurate methods. And, as stated earlier, such an accuracy of the methods employed must not be jeopardized by the interpolation processes they may partly rely on. This implies that the interpolation techniques to be used are such that, once they are applied to a given aeroacoustic signal, they degrade it in a very minimal way. Now, as was also recalled, a previous work by the present authors [14] shown how the signal degradation by a given interpolation operator can be characterized and analyzed in a straightforward manner, provided that the interpolation process is sketched as a composition of three successive steps that are:

0. the discretization of the signal associated continuous function, $f(\cdot)$, onto a so-called *donor* grid, resulting in a discretized function, $f_d(\cdot)$,
1. the reconstruction of a continuous function approximating $f(\cdot)$, with the help of an interpolation operator, $\mathcal{I}[f_d](\cdot)$, and
2. the projection of the reconstructed function $\mathcal{I}[f_d](\cdot)$ onto a so-called *receiver* grid.

In the following, the expression *interpolation process* indicates the composition of the three previous steps. On another hand, the term *interpolation* solely refers to step #1, that is, the operation that reconstructs the discrete function $f_d(\cdot)$ into an approximated continuous function $\mathcal{I}[f_d](\cdot)$. When considering only such step #1, one can show [14] that its associated *interpolation* operation degrades the original signal of function $f(\cdot)$ following two ways:

1. The degradation of correct information, through the alteration of that part of the signal which falls in the higher part of spectrum (in terms of wavenumbers).
2. The creation of incorrect information, through the generation of spurious contents (or modes), which are also of high wavenumber.

One can thus conclude that the interpolated (continuous) signal, $\mathcal{I}[f_d](\cdot)$ will be accurate only over the low- and mid-frequency ranges (in terms of wavenumbers). The point is that, as can also be shown [14], when such signal will be projected onto a given receiver grid (step #2), another side-effect can occur, depending on the ratio between the donor and the receiver respective discretizations: indeed, any of the signal components that is to be under-resolved on the receiver grid will be aliased back into the low- and mid-level frequency ranges. Therefore, at the end, once it will have been successively (i) discretized onto a donor grid, (ii) interpolated from the latter, and then (iii) projected onto a receiver one, a given aeroacoustic signal may end up being entirely degraded, that is, altered over its whole spectrum. In particular, such degradation of the signal will closely depend on the total amount of spurious modes that will have been incorrectly generated, and then further aliased. In other words, the signal degradation to be induced by a given interpolation process may be strongly driven by both the spuriousing (or spurious mode generation) and the subsequent aliasing phenomena it is characterized by.

4. Spectral-like Optimization of Interpolation Schemes

With the view of preventing at best aeroacoustic signals to be degraded by interpolation, some authors have proposed innovative interpolation schemes (either of centered [2, 10] or noncentered [10, 12] nature), which were optimized following a spectral-like strategy, that is to say, in the wavenumber space. Indeed, such so-called *spectral-like* optimization approach aims at enhancing the scheme's ability to preserve the acoustic dispersion/dissipation properties, by minimizing the error it induces on the spectral components of any given harmonic signal.

4.1. Spectral-Like Optimization of Centered Interpolation Schemes

In order to optimize centered interpolation schemes following a spectral-like strategy, one can refer to works by Tam and Kurbatskii [10].

4.1.1. Spectral-like Optimization of Centered Interpolation Schemes: Principle

Indeed, the spectral-like optimization proposed in [10] consists in a minimization of the integrated error that is to be made by a given interpolation scheme on a single Fourier component of the form $f(x) = e^{i\alpha x}$:

$$E(x) = \int_0^\kappa |e^{i\alpha x} - \mathcal{I}[e^{i\alpha x}]|^2 d(\alpha\Delta x_1). \quad (4)$$

In the above, κ indicates the optimization parameter, which determines the frequency range interval over which minimizing the integrated error, with that interval covered by all wavenumbers α . Now, by making use of Equation (1), one can explicitly express the integrated error associated with any given scheme:

$$E(x) = \int_0^\kappa \left| e^{i\alpha\eta\Delta x_1} - \sum_{j=J_{min}}^{J_{max}} S_j(\eta) e^{i\alpha j\Delta x_1} \right|^2 d(\alpha\Delta x_1). \quad (5)$$

where $\eta = x/\Delta x_1 - n$ and $x \in [n\Delta x_1, (n+1)\Delta x_1[$, implying $\eta \in [0, 1[$. Based on that, one can then identify which set of interpolation coefficients (S_j) is the optimal one, that is, the one that will ensure a minimal integrated error.

In addition to such requirement for a minimal integrated error, the interpolation operator coefficients (S_j) are also imposed a specific constraint, so that no error is made on the zero-wavenumber component:

$$\left| 1 - \sum_{j=J_{min}}^{J_{max}} S_j(\eta) \right| = 0, \quad \forall \eta \in [0, 1[. \quad (6)$$

4.1.2. Spectral-like Optimization of Centered Interpolation Schemes : Effective Efficiency

In [10], various centered interpolation schemes were spectral-like optimized following the procedure described above. All associated sets of interpolation coefficients $S_j(\cdot)$ were determined by considering $\kappa = 1.0$, before the various spectral-like schemes were compared to their standard (i.e. non-optimized) counterparts. Finally, based on the observations made, the relevance of the spectral-like optimization process was discussed by the authors, their main conclusion being that, regarding centered interpolations, spectral-like optimized schemes exhibit slightly better properties than their standard counterpart.

One can here point out the fact that the referred study did not really address the question of the spurious mode generation, nor of its possible impact on the spectral-like optimization procedure. Indeed, on that stage, the authors simply mentioned that, from the moment the interpolated signal would be used within a LES or a CAA computation, all of its high frequency (and, thus, possibly spurious) contents would likely be filtered out during the calculation, thanks to selective artificial damping or filtering procedures the latter usually relies on.

The point is that, as was discussed above and demonstrated in [14], long before any high frequency component can be filtered out by such procedures, it may have been partly degenerated into spurious and aliased modes polluting the *whole spectrum* [13, 14, 17], simply because of its interpolation and further projection onto the (receiver) grid over which the calculation is conducted. Needless to say, there is not a chance that all spurious contents lying within the low and mid-parts of the spectrum could be suppressed by artificial selective damping or filtering techniques.

As an illustration, let us consider a signal composed of several test functions $f_k(\cdot)$, to be allotted with an identical amplitude but with various wavenumbers k

$$f_k(x) = \cos\left(\frac{k\pi}{16\Delta x_1}x\right) \exp\left(-\left(\frac{x}{16\Delta x_1}\right)^2\right), k \in [0, 14]. \quad (7)$$

Figure 2 depicts the signals spectrum, which was obtained by analytically evaluating and adding all functions $f_k(\cdot)$ Fourier transforms.

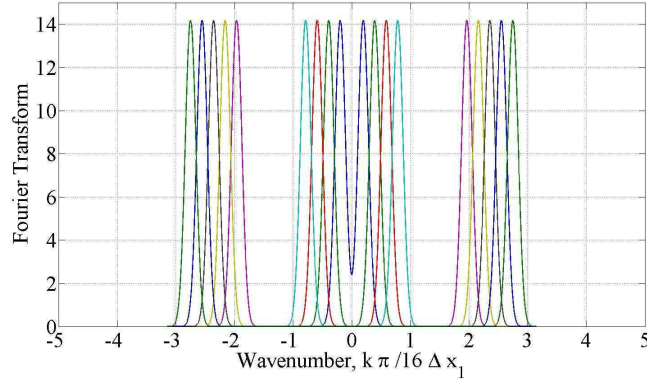


Figure 2: Spectrum of a signal composed with a set of $f_k(\cdot)$ functions associated with various $k \in [0, 14]$ (see Equation (7)).

Let us now interpolate the previous signal from a uniform 1D donor grid of discretization step $\Delta x_1 = 1$ towards a receiver grid associated with a uniform 1D grid of discretization step $\Delta x_2 = (3/5) \times \Delta x_1$. For doing so, let us apply to the signal a 7-point stencil interpolation operator, with the latter centered on each receiver point (i.e. $J_{min} = -3$ and $J_{max} = 3$) so that the interpolation configuration is identical to the one assessed in reference [10]. Figure 3 compares the spectra associated with the interpolated signal obtained via either the standard (Figure 3a) or the spectral-like optimized (Figure 3b) version of such centered 7-point interpolation operator.

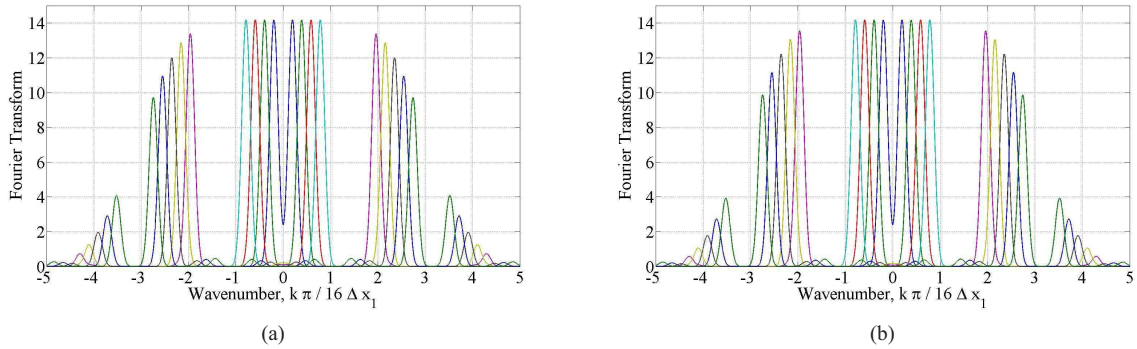


Figure 3: Spectrum of the interpolated signal composed with functions $f_k(\cdot)$, as obtained through a centered 7-point interpolation scheme of either (a) standard or (b) spectral-like optimized [10] types. In the present case, $\Delta x_2 = (3/5) \times \Delta x_1$, with $\Delta x_1 = 1$.

As can be seen, whatever the interpolation operator is of standard or spectral-like optimized kind, it induces the generation of spurious modes *all over the spectrum*. Concerning more particularly the standard operator, one can

observe that the lower part of the spectrum is polluted with spurious modes which amplitude rise up to 3.3% of the original (that is, non-spurious) signal content. Concerning now the spectral-like optimized operator, the situation is roughly similar, with a pollution of the lower part of the spectrum by spurious modes which amplitude rise up to 3.0% of the original content. This clearly shows that, when it comes to minimize the spurious modes generation (and their subsequent aliasing), the spectral-like optimization may not be of great help.

On that stage, one can point out the fact that, although these 3% and some spurious modes amplitude level may appear to be small, they are of relative nature. Indeed, the absolute error level resulting from its spuriousness by interpolation schemes is to be driven by the original signal's high frequency contents magnitude. Now, if one considers how large the magnitude of some typical high-frequency aeroacoustic occurrences (such as aerodynamic ones, e.g. vortices) can be [1, 6], one can legitimately wonder about the effective accuracy of interpolation schemes, when used for solving practical problems involving other components than purely acoustic ones - which is likely to occur in many situations, as, for instance, aerodynamic noise problems [1, 6, 7, 8].

4.2. Spectral-Like Optimization of Noncentered Interpolation Schemes

4.2.1. Spectral-like Optimization of Non Centered Interpolation Schemes - Principle and Effective Efficiency

Following the same approach by Tam and Kurbatskii [10], one can also optimize noncentered interpolation operators in a spectral-like sense, by making use of the same Equation (5) and of its associated constraint of Equation (6). Now, let us repeat the interpolation exercise conducted in the previous section but, this time, with a noncentered operator of same stencil size (7 points) to be defined such that $J_{min} = -5$ and $J_{max} = 1$, that is, with the receiver point located at the donor grid's first interval. As previously done for its centered counterpart, Figure 4 compares the spectra associated with the interpolated signal obtained via either the standard (Figure 4a) or the spectral-like optimized (Figure 4b) version of such noncentered 7-point interpolation operator.

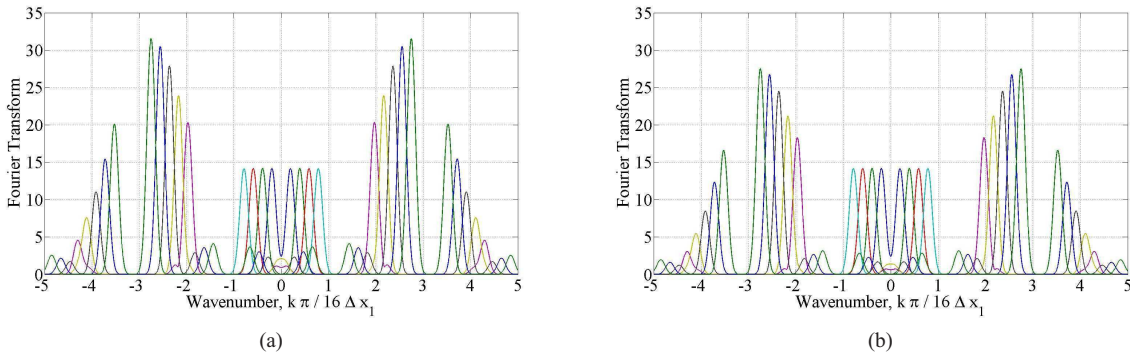


Figure 4: Spectrum of the interpolated signal composed with functions $f_k(\cdot)$, as obtained through a noncentered 7-point interpolation scheme of either (a) a standard or (b) a spectral-like optimized [10] types. In the present case, $\Delta x_2 = (3/5) \times \Delta x_1$, with $\Delta x_1 = 1$.

As can be noticed, for both cases, the spurious modes are more important than the ones resulting from a centered interpolation (see Figure 3). Indeed, over the lower part of the spectrum, the amplitude of the spurious modes generated by such a noncentered standard (resp. spectral-like optimized) interpolation scheme now reaches up to 29.0% (resp. 22.3%) of the original signal's content. In addition, regarding now the upper part of the spectrum, both these noncentered interpolations lead to a strong amplification rate (of almost 100%). This indeed was to be expected since noncentered interpolation schemes are known to be strong amplifiers of high-wavenumber contents [10, 12].

4.2.2. Amplification Controlled Spectral-like Optimization of Noncentered Interpolation Schemes - Principle and Effective Efficiency

With the view of solving such issue, recently, spectral-like optimized interpolation schemes with amplification control have been proposed [12]. The latter schemes are based on an improved optimization approach for which the

interpolation scheme coefficients are also obtained through the minimization of the integrated interpolation error to be made on a single Fourier component of the form $f(x) = e^{i\alpha x}$, but with such error being now defined in a *relative* sense:

$$E(x) = \int_0^\kappa \left| 1 - \frac{\mathcal{I}[e^{i\alpha x}]}{e^{i\alpha x}} \right|^2 d(\alpha \Delta x_1) = \int_0^\kappa \left| 1 - \sum_{j=J_{min}}^{J_{max}} S_j(\eta) e^{i\alpha(j-\eta)\Delta x_1} \right|^2 d(\alpha \Delta x_1). \quad (8)$$

Additional constraints are also imposed, so that the resulting scheme is P th-order accurate:

$$\left| \delta_0^r - \sum_{j=J_{min}}^{J_{max}} S_j(\eta) (j + \eta)^r \right| = 0, \quad \forall \eta \in [0, 1[\text{ and } \forall r \in \{0, 1, 2, \dots, P - 1\}. \quad (9)$$

Finally, as the key idea of such improved optimization technique, a last constraint is applied, which aims at controlling the amplification level of high-wavenumber contents:

$$\left| \int_0^\pi \left(\sum_{j=J_{min}}^{J_{max}} S_j(\eta) e^{i\alpha(j-\eta)\Delta x_1} \right)^{2q} d(\alpha \Delta x_1) - (1 - \beta)^{2q} \right| = 0, \quad (10)$$

with q and β optimization parameters that are to be determined numerically.

As an example, let us consider a noncentered interpolation scheme of 6-point stencil such that $J_{min} = -4$ and $J_{max} = 1$, that is to say, with the receiver point located at the donor grid's first interval. Let us now optimize such scheme following the spectral-like approach with amplification control, by identifying which coefficients minimize Equation (8), with $\kappa = 2\pi/5$, while verifying Equations (9), with $P = 5$.

With the view of assessing the accuracy of the resulting scheme, let us now apply it to the previous signal (composed with test functions $f_k(\cdot)$ of Equation (7)), and compare the spectrum of the interpolated signal with that of its standard counterpart. As can be seen by comparing Figures 5a and 5b, the present spectral-like optimized noncentered scheme does not induce any amplification of the signal's high-wavenumber contents, on the contrary to what happened with its standard counterpart.

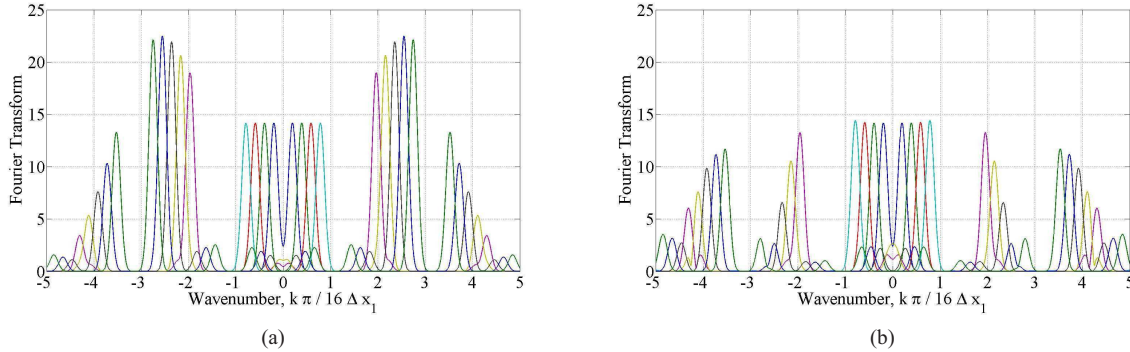


Figure 5: Spectrum of the interpolated signal composed with functions $f_k(\cdot)$, as obtained through a noncentered 6-point interpolation scheme of either (a) standard or (b) spectral-like optimized with amplification control [12] types. In the present case, $\Delta x_2 = (3/5) \times \Delta x_1$, with $\Delta x_1 = 1$.

However, as can also be observed on the same Figure, and still compared to the latter scheme, the present spectral-like optimized noncentered interpolation generates spurious modes of higher amplitudes. More precisely, over the lower part of the signal spectrum, the amplitude ratio between the interpolated (i.e. spurious) and the original contents reaches 18.0% for the standard interpolation scheme, whereas it rises up to 19.0% for the spectral-like optimized and amplification controlled one. In other words, far from having minimized it, the spectral-like optimization process has here *magnified* the spurious mechanism associated with the present noncentered 6-point interpolation scheme.

5. Theoretical Study of the Signal Degradation Induced by Spectral-Like Optimized Interpolation Schemes

All what precedes clearly shows that, whatever they are of centered or noncentered nature, spectral-like optimized interpolation schemes suffer as much as standard ones from the spurious phenomenon. More important, in some situations, the latter can even be magnified by the spectral-like optimization procedure.

With the view of investigating that point further, the present section details a specific analysis that was achieved in order to characterize the signal degradation associated with spectral-like optimized schemes (whatever the latter are of centered or noncentered natures). One can here recall that such analysis directly relies on theoretical developments and outcomes that had been achieved by the present authors in [14], where the signal degradation induced by centered Lagrange interpolation schemes had been characterized thanks to a dedicated analysis of their spurious and subsequent aliasing mechanisms.

5.1. Theoretical Analysis of Centered Spectral-Like Optimized Interpolation Schemes

In order to assess the signal degradations features of centered spectral-like optimized interpolation schemes introduced at Subsection 4.1, let us express their respective and so-called $c_{\Delta x_1}(\cdot)$ function (which characterizes all interpolation features, see Appendix A), and compare it against the one associated with their standard counterpart. For doing so, the various schemes' sets of coefficients $S_j(\cdot)$ are inserted into the $c_{\Delta x_1}(\cdot)$ expression (see Equation (A.3)), which spectrum norm is then determined via a normalized Fourier transform $|\mathcal{F}[c_{\Delta x_1}](\cdot)|/\Delta x_1$.

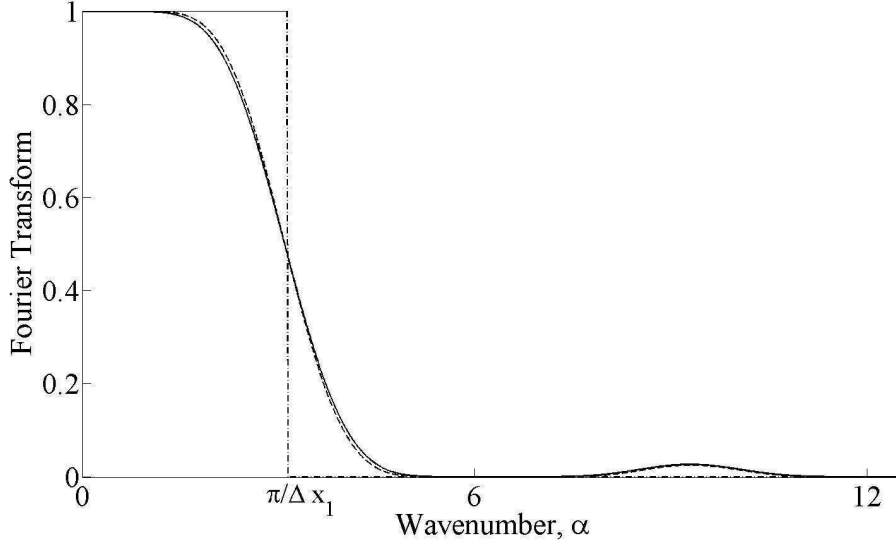


Figure 6: $|\mathcal{F}[c_{\Delta x_1}](\cdot)|/\Delta x_1$. Spectrum norm of $c_{\Delta x_1}(\cdot)$ function associated with a centered 7-point interpolation scheme of either standard (solid line) or spectral-like optimized (dashed line) natures. In dashed-dotted line, the $\mathcal{F}[h_{\Delta x_1}](\cdot)/\Delta x_1$ function, which would correspond to an *ideal* interpolation operator. Please, note that, given the even nature of $|\mathcal{F}[c_{\Delta x_1}](\cdot)|/\Delta x_1$, only half of the spectrum is depicted here.

Figure 6 plots the spectrum norm $|\mathcal{F}[c_{\Delta x_1}](\alpha)|/\Delta x_1$ of the respective $c_{\Delta x_1}(\cdot)$ functions characterizing the centered 7-point interpolation schemes introduced above. As one can see, their standard version exhibits a $c_{\Delta x_1}(\cdot)$ function which spectrum norm (plotted in line) matches the *ideal* interpolation one (in dashed-dotted line) over only one half of the resolved frequency range (given by $\alpha \in]-\pi/\Delta x_1, \pi/\Delta x_1[$). Outside this particular zone, the $c_{\Delta x_1}(\cdot)$ function deviates from the *ideal* interpolation one. As explained in [14], this fact directly translates the degradation to be induced by the present interpolation scheme onto signals it is applied on. More precisely, the progressive loss in amplitude that $|\mathcal{F}[c_{\Delta x_1}](\alpha)|/\Delta x_1$ exhibits over the $\alpha \in]-\pi/\Delta x_1, \pi/\Delta x_1[$ frequency range is directly associated with the alteration of correct information such interpolation scheme will induce onto that part of the signal which is resolved by the donor grid. On another hand, the non identically null values that such $|\mathcal{F}[c_{\Delta x_1}](\alpha)|/\Delta x_1$ function takes over

$\alpha \notin]-\pi/\Delta x_1, \pi/\Delta x_1[$ interval is associated with the creation of incorrect information (i.e. spurious modes generation) such interpolation will induce onto that part of the (continuous) interpolated signal that is not resolved by the donor grid (but that may be aliased when the signal will be projected onto the receiver grid).

By examining further the same Figure 6), one can see that, over the frequency range $\alpha \in]-\pi/\Delta x_1, \pi/\Delta x_1[$, its spectral-like optimization improves the interpolation scheme in a very negligible way, with a $\mathcal{F}[c_{\Delta x_1}](\cdot)/\Delta x_1$ that gets only very slightly closer to the *ideal* interpolation one ($\mathcal{F}[h_{\Delta x_1}](\cdot)/\Delta x_1$, which norm is plotted in dashed-dotted line). This explains the observations made at Section 4.1 about the quasi negligible gain brought to centered interpolation schemes by their spectral-like optimization, which had confirmed the conclusions initially drawn in [10]. On another hand, when considering now the $\alpha \notin]-\pi/\Delta x_1, \pi/\Delta x_1[$ frequency range, one can see that its spectral-like optimization does not really modify (i.e. improve nor degrade) the interpolation scheme, which $\mathcal{F}[c_{\Delta x_1}](\cdot)/\Delta x_1$ function also remains roughly the same. In particular, one can see that the optimization procedure leaves almost unchanged the $\mathcal{F}[c_{\Delta x_1}](\cdot)/\Delta x_1$ function's wave pockets (which, as demonstrated in [14] and recalled in Appendix A, are responsible for the spurious modes generation).

In addition, by observing now the real and imaginary parts of such $\mathcal{F}[c_{\Delta x_1}](\cdot)$ function, one can see that its spectral-like optimization does not improve that much the phase-shift features of the interpolation scheme. As an illustration, Figures 7a and 7b respectively plot the real and the imaginary parts of the phase-shift error E_ϕ to be induced by both schemes, with such quantity defined as:

$$E_\phi(\alpha) = \frac{\mathcal{F}[c_{\Delta x_1}](\alpha)}{\Delta x_1} - \frac{|\mathcal{F}[c_{\Delta x_1}](\alpha)|}{\Delta x_1} e^{i\alpha}. \quad (11)$$

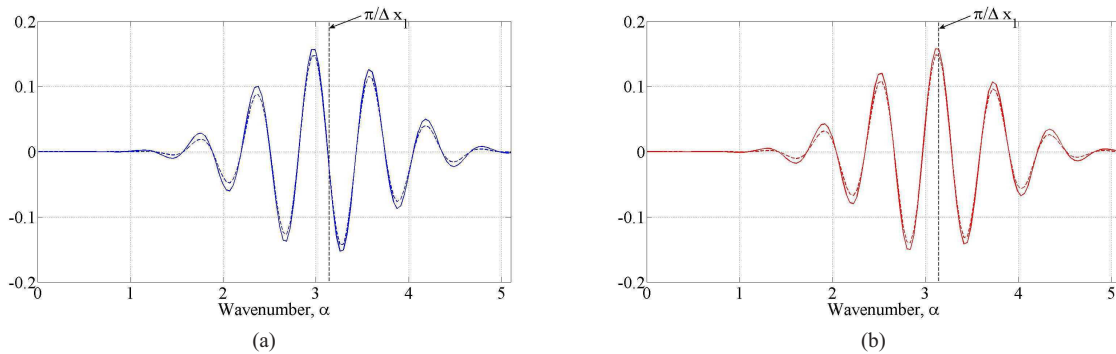


Figure 7: (a) Real and (b) imaginary parts of the phase-shift error E_ϕ induced by centered 7-point interpolation schemes of either standard (solid lines) or spectral-like optimized (dashed lines) natures.

By examining how such error behaves over the higher part of the spectrum, one can conclude that the present 7-point interpolation scheme is likely to induce a phase-shift of high-wavenumber contents, whatever it has been spectral-liked optimized or not. At this stage, one can recall that phase-shift phenomena to be induced by an interpolation can be avoided only if the latter is composed of a centered scheme with an *even* number of stencil points [14] (which was not the case in [10] and, thus, here).

5.2. Theoretical Analysis of Noncentered Spectral-Like Optimized Interpolation Schemes

Analogously to what was done for its centered counterpart, Figure 8 compares the $|\mathcal{F}[c_{\Delta x_1}](\cdot)|/\Delta x_1$ functions associated with both the standard and the spectral-like optimized versions of the noncentered 7-point interpolation (cf Subsection 4.2).

By examining this Figure, one can make several observations and draw various conclusions. First of all, and similarly to what happened to its centered counterpart, the present noncentered standard 7-point interpolation exhibits a $c_{\Delta x_1}(\cdot)$ function which spectrum norm $|\mathcal{F}[c_{\Delta x_1}](\alpha)|/\Delta x_1$ (plotted in line) matches the *ideal* interpolation one (plotted in dashed-dotted line) over approximately half of the resolved frequency range, after what it deviates from it. On that

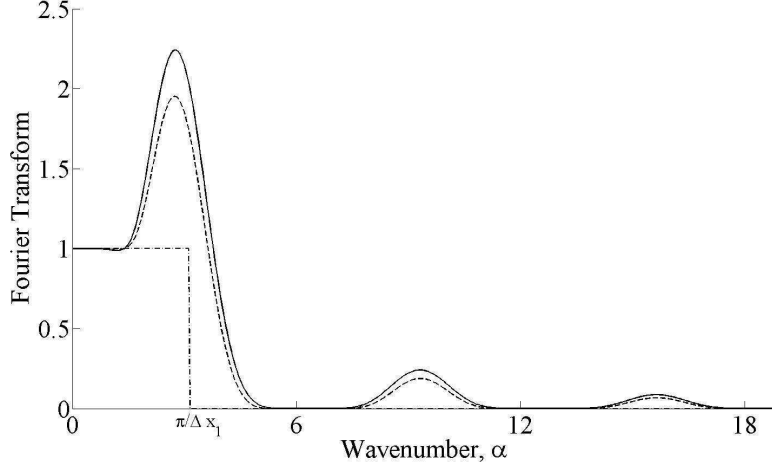


Figure 8: $|\mathcal{F}[c_{\Delta x_1}](\cdot)|/\Delta x_1$. Spectrum norm of $c_{\Delta x_1}(\cdot)$ function associated with noncentered 7-point interpolation of either standard (solid line) or spectral-like optimized (dashed line) nature. In dashed-dotted line, the $\mathcal{F}[h_{\Delta x_1}](\cdot)/\Delta x_1$ function, which would correspond to an *ideal* interpolation operator. Please, note that, given the even nature of $|\mathcal{F}[c_{\Delta x_1}](\cdot)|/\Delta x_1$, only half of the spectrum was depicted here.

point however, and contrarily to what happened in the previous (centered standard scheme) case, such spectrum norm function takes values that largely exceed the unity over a non negligible part of the $\alpha \in]-\pi/\Delta x_1, \pi/\Delta x_1[$ (i.e. resolved) frequency range. This explains why noncentered interpolation schemes such as this one are likely to amplify some of the well-resolved contents of the signal they are applied to. Additionally, over the non resolved frequency range (i.e. $\alpha \notin]-\pi/\Delta x_1, \pi/\Delta x_1[$), this spectrum norm function also exhibits *spurious* wave pockets, which magnitude is more important than in the previous (centered standard interpolation) case. All this indicates that, when applied to a signal, noncentered standard interpolation schemes are not only likely to amplify its high frequency contents, but also to spurious them more importantly than their centered counterpart.

Now, by comparing the previous noncentered standard interpolation $|\mathcal{F}[c_{\Delta x_1}](\alpha)|/\Delta x_1$ curve with that of its spectral-like optimized counterpart (plotted in dashes, on the same Figure 8), one can understand why, although it has some beneficial effects on it, its spectral-like optimization cannot prevent a given noncentered interpolation to possibly (i) amplify and (ii) spurious part of the signal it is applied to. Indeed, as one can see, the scheme spectrum norm $|\mathcal{F}[c_{\Delta x_1}](\alpha)|/\Delta x_1$ is only slightly impacted by the spectral-like optimization process, which leaves it roughly unchanged.

Regarding now the phase-shift phenomenon to be possibly induced by these two noncentered interpolation schemes, Figures 9a and 9b respectively depict the real and imaginary parts of the associated error E_ϕ . Here again, although it is more important than in the case of a centered interpolation, the gain brought by the spectra-like optimization is still insufficient for improving the present noncentered 7-point interpolation scheme in a significant way.

Let us now replace the spectral-like optimized noncentered interpolation previously assessed with its improved version, which is based on the amplification control technique introduced above. Similarly to what was just presented before, Figure 10 compares the $|\mathcal{F}[c_{\Delta x_1}](\cdot)|/\Delta x_1$ functions associated with the noncentered 6-point interpolation (cf Subsection 4.2.2) of either a standard (plotted in lines) or a spectral-like optimized with amplification control (in dashes) nature. By examining this Figure, one can first notice that, compared to its standard counterpart, the present spectral-like optimized with amplification control interpolation exhibits a $c_{\Delta x_1}(\cdot)$ function which spectrum norm $|\mathcal{F}[c_{\Delta x_1}](\alpha)|/\Delta x_1$ rarely exceeds the critical unitary value. This explains why this particular spectral-like optimization technique effectively helps in minimizing the amplification side-effect associated with noncentered interpolations.

On another hand, one can notice that, compared to that of its standard counterpart, such spectrum norm deviates sooner from the ideal interpolation one. This tends to indicate that, compared with the previous spectral-like optimization technique, the present amplification control-based approach may lead noncentered interpolations to induce a

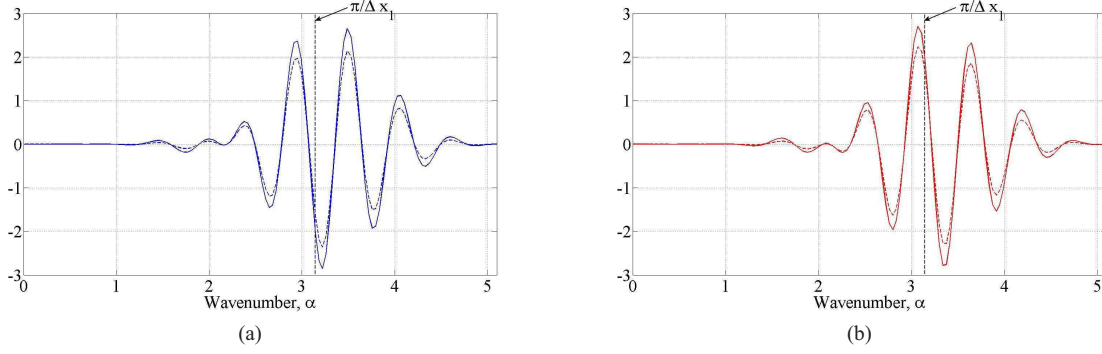


Figure 9: (a) Real and (b) imaginary parts of the phase-shift error E_ϕ induced by noncentered 7-point interpolation schemes of either standard (solid lines) or spectral-like optimized (dashed lines) natures.

higher degradation (in terms of alteration of the correct information) of signal components that are well-resolved. Additionally, concerning now that part of the signal which is not resolved, it appears that the associated signal degradation (in terms of spurious modes generation, this time) is also to be enhanced by this particular spectral-like optimization technique. This, indeed, can be inferred from what happens over the unresolved frequency range ($\alpha \notin]-\pi/\Delta x_1, \pi/\Delta x_1[$), where the $|\mathcal{F}[c_{\Delta x_1}](\cdot)|/\Delta x_1$ function exhibits wavepockets of higher magnitude, compared to the ones associated with the previous spectral-like optimization. Finally, this amplification control-based spectral-like optimization technique is certainly to enhance also the phase shift error by noncentered interpolation schemes, as can be inferred from Figures 11a and 11b.

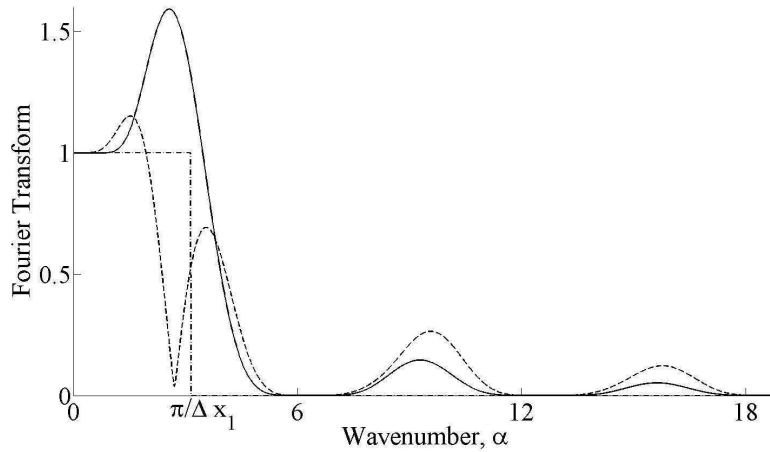


Figure 10: $|\mathcal{F}[c_{\Delta x_1}](\cdot)|/\Delta x_1$. Spectrum norm of $c_{\Delta x_1}(\cdot)$ function associated with a noncentered 6-point interpolation of either standard (solid line) or spectral-like optimized with amplification control (dashed line) nature. In dashed-dotted line, the $\mathcal{F}[h_{\Delta x_1}](\cdot)/\Delta x_1$ function, which would correspond to an *ideal* interpolation. Please, note that, given the even nature of $|\mathcal{F}[c_{\Delta x_1}](\cdot)|/\Delta x_1$, only half of the spectrum is depicted here.

6. Further Insights on the Spurious Modes Generation by Interpolation Schemes

As was assessed and analyzed in the previous Sections, their spectral optimization may slightly enhance the accuracy of interpolation schemes over part of their well-resolved frequency range. However, as was also shown,

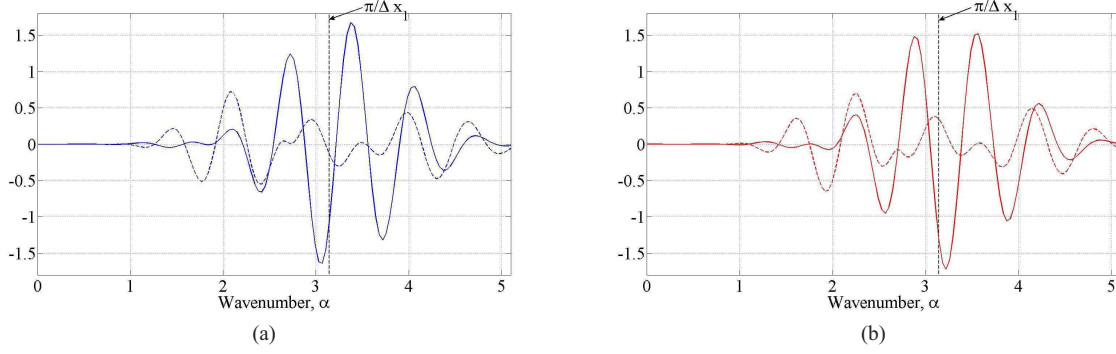


Figure 11: (a) Real and (b) imaginary parts of the phase shift error $\mathcal{F}[c_{\Delta x_1}](\cdot)/\Delta x_1$ induced by noncentered 6-point interpolation schemes of either standard (solid lines) or spectral-like optimized with amplification control (dashed lines) nature

these spectral-like optimization techniques are unable to improve the interpolations' behavior in terms of spurious modes generation.

With the view of (i) better understanding and (ii) potentially removing such inability of spectral-like optimization procedures to minimize the spurious modes generation by interpolation schemes, in the present section, the theoretical investigations conducted above are developed further. The first objective is to derive a particular optimization constraint, to be explicitly related to the minimization of these interpolation errors that are specifically induced by the signal degradation mechanisms. The goal is then to highlight how, because they fail in integrating such specific constraint among their optimization criteria, spectral-like optimized interpolation schemes presented above could not escape degrading signals they are applied to in terms of spurious modes generation.

6.1. Harmonic Analysis - Generic Form

First of all, for preventing an interpolation scheme to degrade a given signal by polluting it with incorrect information, it is first needed to accurately determine *when* and *how* its associated spurious mode generation phenomenon may arise. For doing so, let us apply a given interpolation operator onto a single harmonic component of the form $f(x) = e^{ikx}$, with $k \in]-\pi/\Delta x_1, \pi/\Delta x_1[$. In this particular (harmonic) case, the generic *interpolated signal* expression given by Equation (1) reduces to :

$$\mathcal{I}[e^{ikx}](x) = \sum_{n=-\infty}^{+\infty} \mathbf{1}_{[0,1[}\left(\frac{x}{\Delta x_1} - n\right) \sum_{j=J_{min}}^{J_{max}} S_j\left(\frac{x}{\Delta x_1} - n\right) e^{(n+j)k\Delta x_1}. \quad (12)$$

By taking the Fourier transform of the previous quantity, and after a few manipulations involving, among others, identities of [Appendix A](#), one gets the interpolated signal spectrum:

$$\mathcal{F}[\mathcal{I}[e^{ikx}]](\alpha) = \underbrace{\frac{2\pi\mathcal{F}[c_{\Delta x_1}](\alpha)}{\Delta x_1} \delta(\alpha - k)}_{\text{term} \neq 0 \text{ only for } \alpha = k} + \underbrace{\frac{2\pi\mathcal{F}[c_{\Delta x_1}](\alpha)}{\Delta x_1} \sum_{\substack{n=-\infty \\ n \neq 0}}^{+\infty} \delta\left(\alpha - k - \frac{2\pi n}{\Delta x_1}\right)}_{\text{term} \neq 0 \text{ for various } \alpha \notin]-\pi/\Delta x_1, \pi/\Delta x_1[}, \quad \forall \alpha \in]-\infty, \infty[. \quad (13)$$

In the above expression, the first term (which is non null for $\alpha = k$ only) indeed corresponds to the original signal fundamental frequency.

In the present *harmonic* case, if the interpolation was of *ideal* nature, such interpolated signal spectrum would gather nothing else than this sole component, which expression would then correspond to that of the ideal interpolation, that is, the one associated with $h_{\Delta x_1}(\cdot)$ function, with Equation (13) becoming then:

$$\mathcal{F}[\mathcal{I}[e^{ikx}]](\alpha) = \frac{2\pi\mathcal{F}[h_{\Delta x_1}](\alpha)}{\Delta x_1} \delta(\alpha - k), \quad \forall \alpha \in]-\infty, \infty[, \quad (14)$$

Now, one could ever imagine that, although it is not of ideal nature, a given interpolation could be free of any spurious mode generation, its signal degradation features being then restricted to the sole alteration of correct information. In that case, the previous Equation would become

$$\mathcal{F}[\mathcal{I}[e^{ikx}]](\alpha) = \frac{2\pi\mathcal{F}[c_{\Delta x_1}](\alpha)}{\Delta x_1} \delta(\alpha - k), \quad \forall \alpha \in]-\infty, \infty[. \quad (15)$$

In other words, a sufficient condition for the interpolation to ideally behave in terms of spurious modes generation would be that the second term at right-hand-side of Equation (13) is identically zero. Such term indeed corresponds to all spurious modes that are to be generated over the unresolved part of the frequency range and possibly further aliased back onto its resolved part, when projected onto a receiver grid - all this because of the non ideal nature of the interpolation.²

Therefore, for an optimization technique to effectively minimize the spurious modes generation mechanisms by a given interpolation, it would at least be needed that the optimization process acts in some way onto such second term of the interpolated signal spectrum. This indeed does not seem to be the case with spectral-like optimization approaches, which do not reduce (and, sometimes, even magnify) the amount of spurious modes generated by interpolation schemes, as was numerically assessed in Section 4, and theoretically demonstrated in Section 5.

With the view of investigating that point further, in the following, the harmonic analysis that was here conducted is compared with the (somehow more restrictive) one on which spectral-like optimizations were originally based.

6.2. Harmonic Analysis - Alternative Form

First, let us express Equation (12) in an alternative manner, by considering that $x \in [n\Delta x_1, (n+1)\Delta x_1[$ for a given $n \in \mathbb{N}$. Introducing now the variable change $\eta(x) = x/\Delta x_1 - n$, one gets:

$$\mathcal{I}[e^{ikx}](x) = \underbrace{\left[\sum_{j=J_{min}}^{J_{max}} S_j(\eta) e^{ik\Delta x_1(j-\eta)} \right]}_{T_F(k\Delta x_1, \eta)} e^{ikx}, \quad \eta \in [0, 1[. \quad (16)$$

In the previous expression, the term into brackets corresponds to the interpolation's *local* transfer function, here defined as $T_F(\cdot, \cdot)$. An ideal interpolation scheme would obviously be characterized by a unitary local transfer function, that is $T_F(k\Delta x_1, \eta) = 1, \forall k \in]-\pi/\Delta x_1, \pi, \Delta x_1[$ and $\forall \eta \in [0, 1[$. This, however, is never achieved in practice, and $T_F(k\Delta x_1, \eta) \neq 1$ for some harmonic components of high wavenumber k in $]-\pi/\Delta x_1, \pi, \Delta x_1[$. The principle of spectral-like optimization techniques is indeed to determine the optimal set(s) of $S_j(\cdot)$ such that the T_F -associated integrated error can be minimized over a given frequency range $[-k, k] \subset]-\pi/\Delta x_1, \pi/\Delta x_1[$ (see, for instance, Equations (4) and (8)).

Now, submitting Equation (16) to a Fourier transform, one can relate the interpolation's spectrum with that of its local transfer function:

$$\mathcal{F}[\mathcal{I}[e^{ikx}]](\alpha) = \mathcal{F}[T_F](k\Delta x_1, \alpha - k), \quad \forall \alpha \in]-\infty, \infty[. \quad (17)$$

Finally, by making use of Equation (13), one can express the latter interpolation's local transfer function spectra in terms of the $c_{\Delta x_1}(\cdot)$ function:

$$\mathcal{F}[T_F](k\Delta x_1, \alpha - k) = \underbrace{\frac{2\pi\mathcal{F}[c_{\Delta x_1}](\alpha)}{\Delta x_1} \delta(\alpha - k)}_{\text{term} \neq 0 \text{ only for } \alpha = k} + \underbrace{\frac{2\pi\mathcal{F}[c_{\Delta x_1}](\alpha)}{\Delta x_1} \sum_{\substack{n=-\infty \\ n \neq 0}}^{+\infty} \delta\left(\alpha - k - \frac{2\pi n}{\Delta x_1}\right)}_{\text{term} \neq 0 \text{ for various } \alpha \notin]-\pi/\Delta x_1, \pi/\Delta x_1[}. \quad (18)$$

²All of the theoretical results established here were derived with respect to interpolation, i.e under the assumption that Equation (1) represents an interpolation operator. They can however be readily extended to extrapolation operators providing that assumptions made on intervals of j and n do not question the applicability of the Signal Theory's theorems used here. One can thus infer that extrapolation processes are as likely as interpolation ones to suffer from the spuriousness (and its subsequent aliasing) side-effect.

Considering now what was discussed in Section 6.1, one can conclude that a *spurious modes-free* interpolation scheme would require that the second term at the right-hand-side of Equation (18) is null, that is to say, its local transfer function spectrum should be solely composed of the original signal's fundamental frequency:

$$\mathcal{F}[T_F](k\Delta x_1, \alpha - k) = \frac{2\pi\mathcal{F}[c_{\Delta x_1}](\alpha)}{\Delta x_1}\delta(\alpha - k), \quad \forall \alpha \in]-\infty, \infty[. \quad (19)$$

Needless to say, any optimization procedure that seeks at improving interpolations should integrate this kind of condition, such that resulting interpolation schemes effectively behave better than standard ones, in terms of spurious modes generation³ This was not the case for spectral-like optimization techniques detailed above.

On that stage, however, it is important to underline that the previous identity can be verified by *any* interpolation scheme, from the moment it is used *under specific conditions*. As an example, whenever the interpolation's transfer function associated with the donor and receiver grids is a function of $k\Delta x_1$ only, i.e. $T_F(k\Delta x_1, \eta) = g(k\Delta x_1)$, one can write

$$\mathcal{F}[T_F](k\Delta x_1, \alpha - k) = g(k\Delta x_1)\delta(\alpha - k), \quad \forall \alpha \in]-\infty, \infty[. \quad (20)$$

In such a situation, no creation of incorrect information (i.e. spurious mode generation) can be induced by the interpolation scheme, which signal degradation is therefore restricted to the sole alteration (i.e. dissipation, amplification or dispersion) of the signal original components. In other words, *whatever its interpolation basis $S_f(\cdot)$ is, a given interpolation may see its spurious mode generation features blocked* from the moment its associated local transfer function, $T_F(k\Delta x_1, \eta)$, is function of the dimensionless wavenumber, $k\Delta x$, only. In other words, whenever a given interpolation is assessed under such kind of special circumstances, its associated spuriousing phenomena remains *ineffective*. In particular, this is what happened with the validation cases of spectral-like optimization techniques provided in [10, 12], as is shown in the next Section.

7. On the Relative Validity of Validation Exercises Proposed for Spectra-Like Optimized Interpolation Schemes

Indeed, at this stage, it is legitimate to wonder how spectral-like optimized schemes might misbehave, if one consider the validation exercises with which such schemes had been originally assessed in [10, 12].

With the view of answering such question, thereafter, the particular configurations used by their respective authors for validating the spectral-like optimized schemes they proposed [10, 12] are investigated. The objective here is to assess how far these validation cases were likely to reveal (or not) the spurious noise generation (and subsequent aliasing) that spectral-like optimized schemes appear to be subjected to.

7.1. Optimized Extrapolation and Interpolation Schemes for Immersed Boundary Conditions

In [10], an Immersed Boundary Condition (IBC) was proposed, for which spectral-like optimized interpolation and extrapolation schemes were developed. Figure 12 sketches in 1D the IBC principle, thanks to which a signal known onto a set of donor grid points can be extrapolated towards a non-coincident wall point η . Based on such wall extrapolated value, the boundary condition is then enforced via the last and so-called ghost point of the grid. One can here notice that, in this particular 1D case, the receiver grid is degenerated, gathering the sole wall point of relative coordinate η .

Let us now consider that a given harmonic signal of dimensionless wavenumber $k\Delta x_1$ propagates on such 1D grid, and is thus to be extrapolated onto the wall points as it approaches the boundary. In such a purely *harmonic* case, the extrapolated signal spectrum is simply given by the extrapolation scheme transfer function $T_F(k\Delta x_1, \eta)$, for a well-defined η . It is obvious that such transfer function depends on $k\Delta x_1$ *only* and, thus, that Equation (20) is automatically verified, meaning that *no spurious modes generation can occur*. Therefore, in this particular case, the signal degradation only consists in the possible alteration of well-resolved components (i.e. those such that $k \in]-\pi/\Delta x_1, \pi, \Delta x_1[$); a configuration for which the spectral-like optimization can effectively helps.

³One can here precise that, based on all these outcomes, a specific study was conducted, which resulted in developing an innovative optimization technique for interpolations of minimal spurious modes generation. This will be the matter of another article by the present authors.

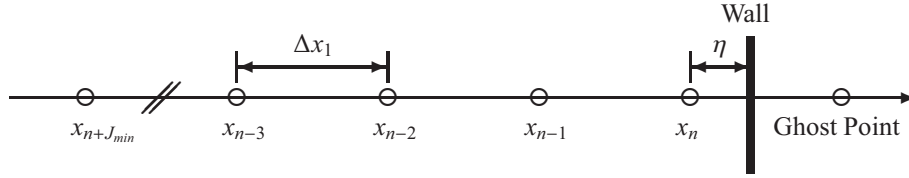


Figure 12: 1D configuration illustrating the Immersed Boundary Condition of [10].

Now, let us consider the 2D-curvilinear equivalent of the previous case with a curved solid wall sunk within a bi-dimensional Cartesian homogeneous grid of discretization steps Δx and Δy , as depicted in Figure 13. In this case, the IBC treatment [18] still begins with a 1D extrapolation (i.e. along x -lines) of the propagated signal towards the wall points A and B . From the latter points, the segment \overline{AB} approximating the curve \widehat{AB} is drawn, from which the point C such that $\overline{CG_B} \perp \overline{AB}$ is then determined. Finally, once the extrapolated signal of A - and B -wall points has been interpolated onto it, such point C allows enforcing the boundary condition at ghost point G_B . Needless to say, since the previous approach relies on a linear approximation of curve segments (\overline{AB} vs \widehat{AB}), the denser the mesh is, and the better the IBC will behave. Although necessary, such condition may not be sufficient for ensuring that this particular IBC technique is accurate enough, as will be shown below.

Indeed, let us consider again a harmonic signal of dimensionless wavenumber $k\Delta x$ that propagates in the x -direction, and that is to be extrapolated as it reaches A and B wall points. As previously, in such a *harmonic* case, the extrapolated signal spectrum at point A (resp. B) is given by the extrapolation schemes transfer function $T_F(k\Delta x, \eta_A)$ (resp. $T_F(k\Delta x, \eta_B)$). Contrarily to what happened before, however, such function is *no longer dependent of $k\Delta x$ only*, that is, will not deliver the same value, depending on which wall point it is considered. Therefore, Equation (20) may not be verified, meaning that *spurious modes generation can occur*, depending on the signal dimensionless wavenumber $k\Delta x$. As an example, the spectral-like optimized extrapolation scheme proposed in [18] was designed to accurately predict wavenumbers up to 8 points-per-wavelength (PPW) [18]. One can thus consider that for signal components of more than 8 PPW, $T_F(k\Delta x, \eta_A) \cong T_F(k\Delta x, \eta_B)$, that is, the spurious modes to be generated are negligible.

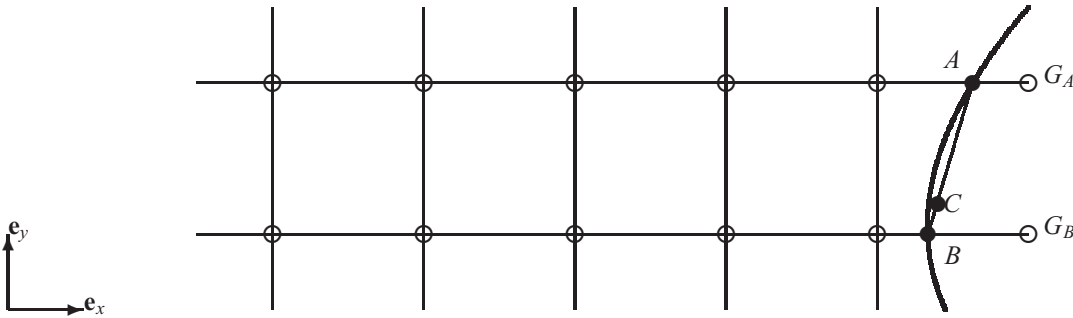


Figure 13: 2D curvilinear extension of the 1D configuration depicted in Figure 12. Points B (resp. A) corresponds to the intersection between the wall and the donor grid line, while G_B (resp. G_A) is the ghost point where the boundary condition is to be enforced, via point C (such that $\overline{CG_B} \perp \overline{AB}$).

On another hand, for signal components such that $k\Delta x$ is less than 8 PPW, the assumption $T_F(k\Delta x, \eta_A) \cong T_F(k\Delta x, \eta_B)$ no longer holds, that is, spurious modes to be generated have no reason to be negligible. In particular, since the extrapolation scheme is here of noncentered nature, one can expect both high-wavenumber contents and spurious modes to be amplified, a thing that the signal dissipation to be possibly induced by the $A + B \rightarrow C$ linear interpolation step may be far insufficient to remedy.

From a more global point-of-view, it is important to notice that the latter situation may occur *whatever the frequency of the signal is*, from the moment the later propagates in another direction than the x -axis. Indeed, in those

cases where the propagating direction deviates from the grid lines one, the signal wavenumber k decomposes itself into k_x and k_y components (with $k = \sqrt{k_x^2 + k_y^2}$), with the latter components taking any value between 0 and k . On another hand, for the extrapolation stage not to generate spurious modes, the criteria enunciated above for $k\Delta x_1$ is now to be verified by $k_x\Delta x$ and $k_y\Delta y$. Therefore, unless both conditions are verified at the same time, the IBC extrapolation stage is likely to generate spurious modes.

7.2. Optimized Interpolation Schemes and Overlapping Grids

In [12], various spectral-like optimized interpolations were assessed, thanks to a dedicated test case that relied on two *1D identical and homogeneous* grids overlapping each other. On the first grid, a signal consisting in a low-wavenumber wave-packet was convected through the *1D* convection equation, while being artificially polluted with a spurious mode given by a low-amplitude high-wavenumber wave-packet, to be forced through the convection equation source term. Such polluted signal was then transferred from the first to the second grid via noncentered spectral-like optimized interpolation schemes, either with or without amplification control. On the other hand, the data transfer to occur from the second to the first grid was carried out via a centered Lagrange interpolation.

The authors shown that, when the interpolation stage was conducted with noncentered spectral-like optimized schemes without amplification control, the signal saw its high-frequency mode being amplified until the simulation blew up. On another hand, when noncentered amplification control-based optimized interpolations were used instead, the simulation remained stable, and delivered the expected results.

On that stage, however, one can again underline that such a validation exercise does not seem to have been of sufficient generality for allowing to properly assess *all* side-effects by interpolations, such as the spurious mode generation. More precisely, the simple fact that such interpolation operation was conducted between two translated *identical and homogeneous* grids prevented it from generating any spurious mode. Indeed, here again, the interpolated signal was defined by the interpolation scheme's transfer function, which - in such particular configuration - was dependent of the dimensionless wavenumber only. As for the previous case (see Section 7.1), this implied that Equation (20) was automatically verified, that is, *no spurious modes generation could occur*.

In order to illustrate that point from a more global perspective, let us extend in two dimensions the particular *1D* configuration proposed in [12]. For doing so, let us consider two identical homogeneous Cartesian *2D* grids, to be simply translated along both x - and y -directions by a vector (η_x, η_y) :

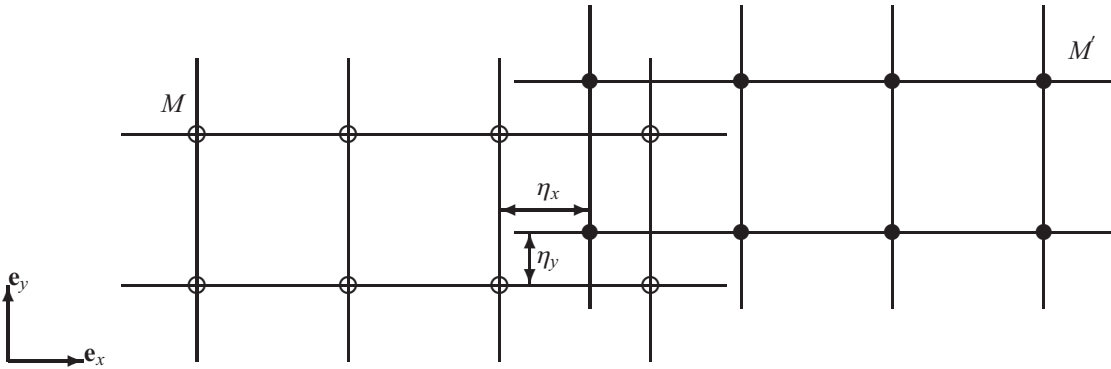


Figure 14: *2D* extension of the *1D* configuration proposed in [12], with two *identical and homogeneous* Cartesian grids overlapping each other, while departing from a vector (η_x, η_y) .

Now, let us consider that one transfers a harmonic signal from one grid to the other, by making use of interpolations. Whatever the x - (resp. y -) interpolation scheme to be used is, for all receiver points and for all $k_x \in]-\pi/\Delta x, \pi/\Delta x[$ (resp. $k_y \in]-\pi/\Delta y, \pi/\Delta y[$), the interpolation's transfer function is always dependent of the dimensionless wavenumber $k\Delta x$ (resp. $k\Delta y$) only, taking an identical $T_F(k\Delta x, \eta_x)$ (resp. $T_F(k\Delta y, \eta_y)$) value. As a result, for both directions, no spurious modes can be generated by the interpolation process, which signal degradation

effect is then solely composed of all dissipation (for centered schemes) or amplification (for noncentered schemes) phenomena to occur over the higher part of the frequency range (besides the dispersion phenomenon).

On another hand, it is clear that the improvements brought by the spectral-like optimized interpolation schemes may no longer hold from the moment the above *homogeneous* Cartesian grids are replaced with *heterogeneous* (e.g. stretched) ones, which is likely to occur when realistic problems are to be addressed. Indeed, in that case, the interpolation's transfer functions may no longer depends on the dimensionless wavenumber only, since it *also* varies with the local (η_x, η_y) donor-to-receiver grids shift⁴. Therefore, the interpolation process is likely to induce some spurious mode generation (and subsequent aliasing) over that part of the frequency range which would not meet specific criteria (see [14]).

8. Conclusion

The present work focused on the effective accuracy of interpolation schemes to be used within a Computational Acoustic context. With that view, various interpolation schemes of either high-order standard or spectral-like optimized nature were assessed. More precisely, we focused here on the degradation such interpolation schemes may induce onto aeroacoustic signals they are applied to, once integrated within an interpolation *process*.

First, it was here shown that such signal degradation by a given interpolation operator consists not only in the (i) alteration (via either dissipation, amplification or dispersion effects) of the signal's original contents, but also in their (ii) corruption via a spurious and its subsequent aliasing phenomena. It was then shown how interpolation schemes, whatever they are of centered or noncentered kind, are thus likely to degrade aeroacoustic signals they are applied to. It was also proven that, although their spectral-like optimization may effectively improve interpolation schemes in some way, it cannot really help in minimizing their signal degradation features, whatever the latter are associated with an alteration or a corruption of the interpolated contents. On that stage, it was shown how spectral-like optimized interpolation schemes assessed here had been initially validated by their authors on the basis of specific test cases, which particular set up prevented the spurious modes generation to occur.

All these outcomes were drawn thanks to assessment exercises relying on academic test cases, as well as to theoretical developments based on an already existing (and published) dedicated formalism by the present authors. In particular, the latter formalism allowed here to determine (i) what criteria shall better be respected by interpolation schemes for not generating spurious modes, and (ii) how spectral-like optimization techniques failed in integrating such criteria within their optimization constraints.

On that stage, one can notice that, thanks to the generality of all theoretical ingredients it relies on, the present study could easily be extended to other types of interpolation schemes (e.g. spline interpolations). In addition, part of these theoretical outcomes, such as the $c_{\Delta x}(\cdot)$ function formalism, could be of great help for developing optimization procedures that could ensure to interpolation *process* a low signal degradation level. In particular, within another framework, an innovative and non spectral-based optimization procedure of that kind was developed by the present authors, before it was validated via a direct application to academic and realistic test cases. This subject will constitute the matter of a future article.

Appendix A. The Interpolation Under the Point of View of the Signal Theory

Let us consider a square-integrable function $f : \mathbb{R} \mapsto \mathbb{R}$. According to the convention used in the present study, its Fourier transform is given by:

$$\mathcal{F}[f](\alpha) = \int_{-\infty}^{+\infty} f(x)e^{-i\alpha x} dx, \quad (\text{A.1})$$

⁴On that stage, it is important to notice that, concerning each receiver point's relative location with respect to its immediate surrounding donor points, there is a perfect bijection between the physical domain (where the donor mesh is possibly heterogeneous and curvilinear) and the computational one (where it is, on the contrary, of homogeneous and Cartesian nature). This being verified, any consideration that can be made in the physical domain about the relative location (and, thus, the local transfer function $T_F(\cdot, \cdot)$) finds a direct and immediate translation in the computational one, where the present theoretical analysis and outcomes apply.

where α is a given wavenumber. The fundamental result of the Signal Theory states that, if the support of $\mathcal{F}[f](\cdot)$ is included in $\left] \frac{-\pi}{\Delta x_1}, \frac{\pi}{\Delta x_1} \right]$, then the function f can be written as a convolution product [13]:

$$f(x) = \sum_{n=-\infty}^{+\infty} f(n\Delta x_1)h_{\Delta x_1}(x - n\Delta x_1) = f_d * h_{\Delta x_1}(x), \quad (\text{A.2})$$

where $f_d(x) = \sum_{n=-\infty}^{+\infty} f(n\Delta x_1)\delta(x - n\Delta x_1)$ is the discretized form of $f(\cdot)$ and $h_{\Delta x_1}(x) = \frac{\sin(\pi x/\Delta x_1)}{\pi x/\Delta x_1}$. Considering now that interpolating a function can be seen as reconstructing it with the help of specific interpolation basis, it appears that $h_{\Delta x_1}(\cdot)$ would indeed constitute an *ideal* interpolation. However, in Equation (A.2) the sum over n is infinite and cannot thus be truncated arbitrarily. Therefore, it is more indicated to replace $h_{\Delta x_1}(\cdot)$ by a finite set of interpolators, $c_{\Delta x_1}(\cdot)$, to be defined as [8]:

$$c_{\Delta x_1}(x) = \sum_{j=J_{\min}}^{J_{\max}} \mathbf{1}\left(\frac{x}{\Delta x_1} + j\right) S_j\left(\frac{x}{\Delta x_1} + j\right). \quad (\text{A.3})$$

In this case, Equation (1) becomes [13]:

$$\mathcal{I}[f](x) = \sum_{n=-\infty}^{+\infty} f(n\Delta x_1)c_{\Delta x_1}(x - n\Delta x_1) = f_d * c_{\Delta x_1}(x). \quad (\text{A.4})$$

Thanks to the presence of the identity function into Equation (A.3), $\mathcal{I}[f](x)$ has a compact support for a given x , which means that, in practice, the sum over n can be safely truncated. However, one can remark that the interpolation basis $S_j(\cdot)$ shall better be chosen such that $c_{\Delta x_1}(\cdot)$ is close enough to $h_{\Delta x_1}(\cdot)$.

Given that interpolating a given function corresponds to a convolution between the latter and the $c_{\Delta x_1}$ function, the interpolation process can be simply sketched as the following successive steps:

0. discretization of $f(\cdot)$ on the donor grid,

$$f_d(x) = \sum_{n=-\infty}^{+\infty} f(n\Delta x_1)\delta(x - n\Delta x_1), \quad (\text{A.5})$$

1. interpolation of the discretized function, f_d ,

$$\mathcal{I}[f](x) = f_d * c_{\Delta x_1}(x), \quad (\text{A.6})$$

2. projection of the interpolated function onto the receiver grid,

$$\mathcal{I}[f]_d(x) = \sum_{n=-\infty}^{+\infty} \mathcal{I}[f](n\Delta x_2)\delta(x - n\Delta x_2). \quad (\text{A.7})$$

Where the subscript $i \in \{1, 2\}$ associated with a given variable indicates on which grid it is considered (donor, $i = 1$, or receiver, $i = 2$).

Taking the Fourier transform of Equations (A.5)-(A.7) leads to, respectively:

$$\mathcal{F}[f_d](\alpha) = \frac{1}{\Delta x_1} \sum_{m_1=-\infty}^{\infty} \mathcal{F}[f]\left(\alpha - \frac{2\pi m_1}{\Delta x_1}\right), \quad (\text{A.8})$$

$$\mathcal{F}[\mathcal{I}[f]](\alpha) = \mathcal{F}[f_d](\alpha) \times \mathcal{F}[c_{\Delta x_1}](\alpha), \quad (\text{A.9})$$

$$\mathcal{F}[\mathcal{I}[f]_d](\alpha) = \frac{1}{\Delta x_2} \sum_{m_2=-\infty}^{+\infty} e^{-i\frac{2\pi m_2}{\Delta x_2}d} \mathcal{F}[\mathcal{I}[f]]\left(\alpha - \frac{2\pi m_2}{\Delta x_2}\right), \quad (\text{A.10})$$

or, equivalently,

$$\mathcal{F}[I[f]_d](\alpha) = \frac{1}{\Delta x_1 \Delta x_2} \sum_{m_2, m_1 = -\infty}^{\infty} e^{-i \frac{2\pi m_2}{\Delta x_2} d} \mathcal{F}[f] \left(\alpha - \frac{2\pi m_1}{\Delta x_1} - \frac{2\pi m_2}{\Delta x_2} \right) \times \mathcal{F}[c_{\Delta x_1}] \left(\alpha - \frac{2\pi m_2}{\Delta x_2} \right). \quad (\text{A.11})$$

Equation (A.11) contains all the interpolation features, like the mechanisms responsible for (i) the degradation of high-wavenumber contents and (ii) the spurious modes generation and aliasing. By a proper study of such equation, one can draw several conclusions, which only the two principal are enumerated here (for further details, see [14]).

- Over the resolved frequency range, i.e. $\alpha \in]-\pi/\Delta x_1, \pi/\Delta x_1[$, the signal will see its norm $|\mathcal{F}[f](\alpha)|$ (i) conserved if $\frac{\mathcal{F}[c_{\Delta x_1}](\alpha)}{\Delta x_1} \cong 1$, (ii) reduced if $\frac{\mathcal{F}[c_{\Delta x_1}](\alpha)}{\Delta x_1} < 1$, (iii) magnified if $\frac{\mathcal{F}[c_{\Delta x_1}](\alpha)}{\Delta x_1} > 1$.
- Whenever $\frac{\mathcal{F}[c_{\Delta x_1}](\alpha)}{\Delta x_1} \neq 0$ over the unresolved frequency range, i.e. $\alpha \notin]-\pi/\Delta x_1, \pi/\Delta x_1[$, the signal will see its content polluted by spurious modes.

Appendix B. Phase Shifting Induced by Interpolation Process' Step #2

In the present work, all discretization grids are written as $x_i = n_i \Delta x_i$, where $n_i \in \mathbb{Z}$ and $i \in \{1, 2\}$. However, if one considers a receiver grid that takes the form $x_2 = n_2 \Delta x_2 + d$, where $n_2 \in \mathbb{N}$, $d \neq 0$ and $d \in [-\Delta x_1/2, \Delta x_1/2[$, then a (non unitary) *grid-to-grid dephasing* term, D_ϕ , appears in equation (A.11).

$$D_\phi = e^{-i \frac{2\pi m_2}{\Delta x_2} d}, \quad m_2 \in \mathbb{Z}. \quad (\text{B.1})$$

One can remark that, for $m_2 = 0$, $D_\phi = 1 \forall d$, which means that no grid-to-grid dephasing occurs, even if $d \neq 0$. Therefore, whenever a sampling rate reduction or an interpolation is carried out, only the already frequency-shifted contents (i.e. all aliased modes) will suffer from such grid-to-grid dephasing.

References

- [1] C. K. W. Tam, Computational aeroacoustics: An overview of computational challenges and applications, *Journal of Computational Fluid Dynamics* 18 (6) (2004) 247–567.
- [2] S. E. Sherer, J. N. Scott, High-order compact finite-difference methods on general overset grids, *Journal of Computational Physics* 210 (2) (2005) 459–496.
- [3] S. Redonnet, On the numerical prediction of aerodynamic noise via a hybrid approach - part 1, AIAA Paper 2010-3709.
- [4] S. Redonnet, Simulation de la propagation acoustique en presence d'écoulements quelconques et de structures solides, par resolution numerique des equations d'euler, Ph.D. thesis, Universite Bordeaux I, Bordeaux (Oct. 2001).
- [5] S. Redonnet, D. Lockard, D. Khorrami, M. Choudhari, Cfd-caa coupled calculations of a tandem cylinder configuration to assess facility installation effects, AIAA Paper 2011-2841.
- [6] E. Manoha, C. Herrero, P. Sagaut, S. Redonnet, Numerical prediction of airfoil aerodynamic noise, AIAA Paper 2002-2573.
- [7] M. Terracol, E. Manoha, C. Herrero, E. Labourasse, S. Redonnet, P. Sagaut, Hybrid methods for airframe noise numerical prediction, *Theoretical and Computational Fluid Dynamics* 19 (3) (2005) 197–227.
- [8] G. Desquesnes, M. Terracol, E. Manoha, P. Sagaut, On the use of high order overlapping grid method for coupling in cfd/caa, *Journal of Computational Physics* 220 (1) (2006) 355–382.
- [9] C. K. W. Tam, K. A. Kurbatskii, Multi-size-mesh multi-time-step dispersion-relation-preserving scheme for multiple-scales aeroacoustics problems, *International Journal of Computational Fluid Dynamics* 17 (2) (2003) 119–132.
- [10] C. K. W. Tam, K. A. Kurbatskii, An optimized extrapolation and interpolation method for computational aeroacoustics, AIAA Paper 2001-0282.
- [11] N. Pellers, A. L. Duc, F. Tremblay, M. Manhart, High-order stable interpolations for immersed boundary methods, *International Journal for Numerical Methods in Fluids* 52 (11) (2006) 1175–1193.
- [12] D. Desvigne, O. Mardsen, C. Bogey, C. Bailly, Development of noncentered wavenumber-based optimized interpolation schemes with amplification control for overlapping grids, *SIAM Journal of Scientific Computing* 32 (4) (2010) 2074–2098.
- [13] R. W. Schafer, L. R. Rabiner, A digital signal processing approach to interpolation, *Proceedings of the IEEE* 61 (6) (1973) 692–702.
- [14] G. Cunha, S. Redonnet, On the signal degradation induced by the interpolation and the sampling rate reduction in aeroacoustics hybrid methods, *International Journal for Numerical Methods in Fluids* (DOI: 10.1002/flid.3693) 71 (7) (2013) 910–929.
- [15] J. P. Boyd, *Chebyshev and Fourier Spectral Methods*, Springer-Verlag, 1989.
- [16] P. Schmid, *An Introduction to Computational Fluid Dynamics*, John Wiley and Sons Inc., 2007.
- [17] G. Cunha, S. Redonnet, An innovative interpolation technique for aeroacoustic hybrid methods, AIAA Paper 2011-2754.
- [18] K. A. Kurbatskii, C. K. W. Tam, Cartesian boundary treatment of curved walls for high-order computational aeroacoustics schemes, *AIAA Journal* 35 (1) (1997) 133–140.